

Multi-Quantum-Well Ridge Waveguide Lasers for Tunable External-Cavity Sources

A new multi-quantum-well ridge waveguide laser enhanced for use in a grating-tuned external-cavity source has been developed. The device offers higher output power and wider tunability for improved performance in a new instrument. A core technology has been developed for use in a variety of light-emitting devices.

by Tirumala R. Ranganath, Michael J. Ludowise, Patricia A. Beck, Dennis J. Derickson, William H. Perez, Tim L. Bagwell, and David M. Braun

Tunable laser sources for testing of optical components and subsystems are an important part of a family of lightwave communication test and measurement instruments that HP has developed over the last decade. Currently, HP offers two tunable laser sources: the HP 8167A and HP 8168A.¹ These instruments function in the wavelength windows centered at 1300 nm and 1550 nm.

Custom requirements of test instruments cannot always be met by commercially available lasers. As a result, semiconductor laser development was begun to provide core material and device technologies that would produce suitable optical gain media chips for future tunable laser sources. The laser described in this article is the optical gain medium for the HP 8168C tunable laser source. The same technology forms the basis for other custom optical sources, such as the edge-emitting LEDs discussed in the article on page 43.

There are many different aspects to the development of a custom laser chip: device design, material growth, fabrication, testing, and reliability. Wide tunability and high output power are two very important requirements for the instrument application. The device must also be capable of operation in an external-cavity laser source like the HP 8168C.

A semiconductor laser is an optical oscillator, and like any oscillator, it consists of an optical amplifier (realized in a suitable semiconductor material system) together with feedback (provided by two atomically parallel cleaved facets). There are two classes of semiconductor lasers: gain guided and index guided. They are distinguished by the waveguiding mechanism for the optical field. Gain guided devices are relatively simple to fabricate but have high threshold current and astigmatism of the output beam. Index guided lasers can be more challenging to fabricate but offer low threshold currents, high linearity of output power, and good beam quality.

There are a number of variants of the index guided laser. The most sophisticated involve multiple regrowths of epitaxial material around the waveguide. A ridge waveguide laser,² while still index guided, has no regrowth steps, moderate threshold currents, excellent beam quality, and potentially

high reliability. Ridge structures do not exhibit the best linearity of output power with current drive (as do the best buried structures) and therefore are not suitable for applications such as CATV. But for external-cavity sources, ridge waveguide lasers provide excellent performance.

The amplifying region in the ridge structure allows a single optical mode to propagate while a suitable electron-hole population distribution is maintained by an electrical current. Details such as material composition, layer thickness, and ridge dimensions impact the threshold current, differential quantum efficiency, and far-field divergence angles of the light emanating from the two device facets. The far-field divergence angles determine how efficiently the device can couple to a hybrid grating-tuned external cavity on one side and to a single-mode fiber output on the other. The device threshold current is the point at which the amplifier gain equals the total cavity losses. Useful optical power output is obtained only for currents greater than threshold. Differential quantum efficiency is a measure of the device's ability to convert electrical energy to coherent optical output power, once the injected current exceeds threshold.

Tunability is intimately tied to the electronic band structure of the semiconductor as well as our ability to grow a device's light-emitting region by means of a vapor phase technique known as organometallic vapor phase epitaxy (OMVPE). To operate in an external cavity, a device also needs an antireflection coating. Devices must be reliable, so time-consuming reliability studies are done. Groups of devices are stressed at high temperatures, high currents, or both for many thousands of hours. Also, devices must be tested in chip form and in subassembly module form.³ To anticipate instrument operation a laboratory grating-tuned external cavity is used. This allows a quick look at tunability and output power for a given device.

Semiconductor Laser Device

In Fig. 1 we show a schematic cross section of a ridge waveguide laser. Essential features of our device are a multi-quantum-well active region surrounded by n-type and p-type

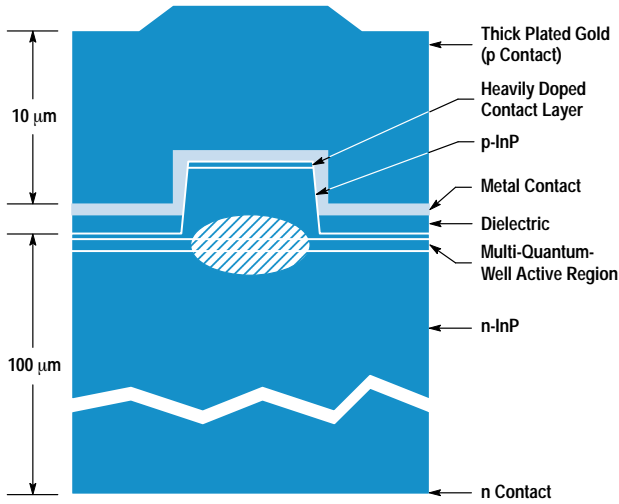


Fig. 1. Ridge waveguide laser cross section.

InP cladding regions. The upper part of the device has an etched ridge whose function it is to confine light laterally, forming a single-mode optical waveguide. With a p ohmic metal contact on the ridge top and an insulator on either side, current is confined to a specific region. The completed device has front and back facets cleaved to form atomically flat and parallel end mirrors. The two end mirrors together with the optical waveguide form an optical cavity. The ridge is typically a few micrometers wide and a few micrometers high, while the completed chip is on the order of 100 micrometers thick and a few hundred micrometers on each side. The p contact has a thick gold pad plated to act as a heat spreader in addition to forming a bond pad. An n contact on the backside of the chip completes the device.

Active Region Design

Absorption, Stimulated Emission, and Optical Gain. In a direct bandgap semiconductor (say, the active region of a laser), an electron from a filled valence band state can absorb an incident photon (of energy $> E_g$, where E_g is the bandgap energy). In the process the electron gets transferred to a conduction band state, leaving behind a vacancy (hole). The absorption rate depends on the incident photon flux and the density of available conduction band states. In the reverse process, stimulated emission, an incoming photon of energy E_p stimulates an electron-hole pair to emit a second in-phase photon (of energy E_p). The stimulated emission rate depends on the incident photon flux, the density of electrons in the conduction band, and the density of holes (at the correct energy) in the valence band. A quantum-mechanical matrix element that measures the strength of the optical coupling between hole states (in the valence band) and electron states (in the conduction band) enters into the calculation for optical absorption and emission states.

It is this stimulated emission process, under conditions of electrical pumping (with a sufficient density of electrons and holes in the conduction and valence band states) that can provide optical gain. When the stimulated emission rate exceeds the (stimulated) absorption rate there is net optical gain. This is generally possible only under high electrical pumping conditions. In addition, an electron from the conduction band can spontaneously emit a photon by recombining

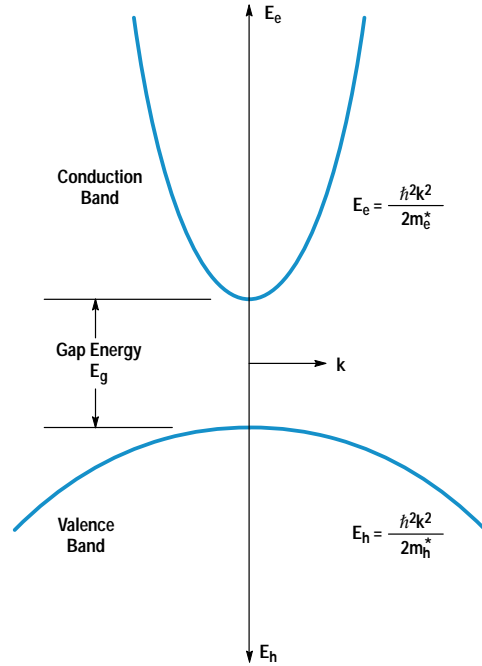


Fig. 2. Parabolic energy E versus crystal momentum k diagram (simplified) for a direct bandgap semiconductor having an energy gap E_g . The difference in curvatures reflects the difference in carrier effective masses for electrons (m_e^*) and holes (m_h^*).

with a hole from a valence band state. This process does not depend on the presence of an incident photon and gives rise to optical noise in laser devices.

Electron/Hole Density of States and Tunability. To gain an appreciation for how optical gain over a broad window arises, a brief examination of electron/hole states in a direct bandgap semiconductor is useful. In a bulk direct bandgap semiconductor, electron and hole states generally exhibit a parabolic relation between energy E and the crystal momentum k (see Fig. 2). In the conduction band,

$$E_e = \frac{\hbar^2 k^2}{2m_e^*},$$

where m_e^* is the electron effective mass, and in the valence band,

$$E_h = \frac{\hbar^2 k^2}{2m_h^*},$$

where m_h^* is the hole effective mass. The electron effective mass is about a factor of 10 smaller than the hole effective mass and this is reflected as a factor of 10 difference in the curvatures of the parabolas in the conduction and valence bands. The three-dimensional density of allowed electron and hole states per unit energy is proportional to \sqrt{E} for a bulk semiconductor. For the case of a very thin ($L_z \approx 10$ nm) layer of the same bulk semiconductor sandwiched between two barrier regions of a higher bandgap material, a structure known as a quantum well, the electron and hole motions are restricted and the allowed energies for motion normal to the layer are quantized and occur at discrete energies (say E_e^1, E_e^2, \dots) determined by the dimension L_z . Motion in the plane of the film is not restricted and allowed energy states form a continuum. The result is a constant density of states for both

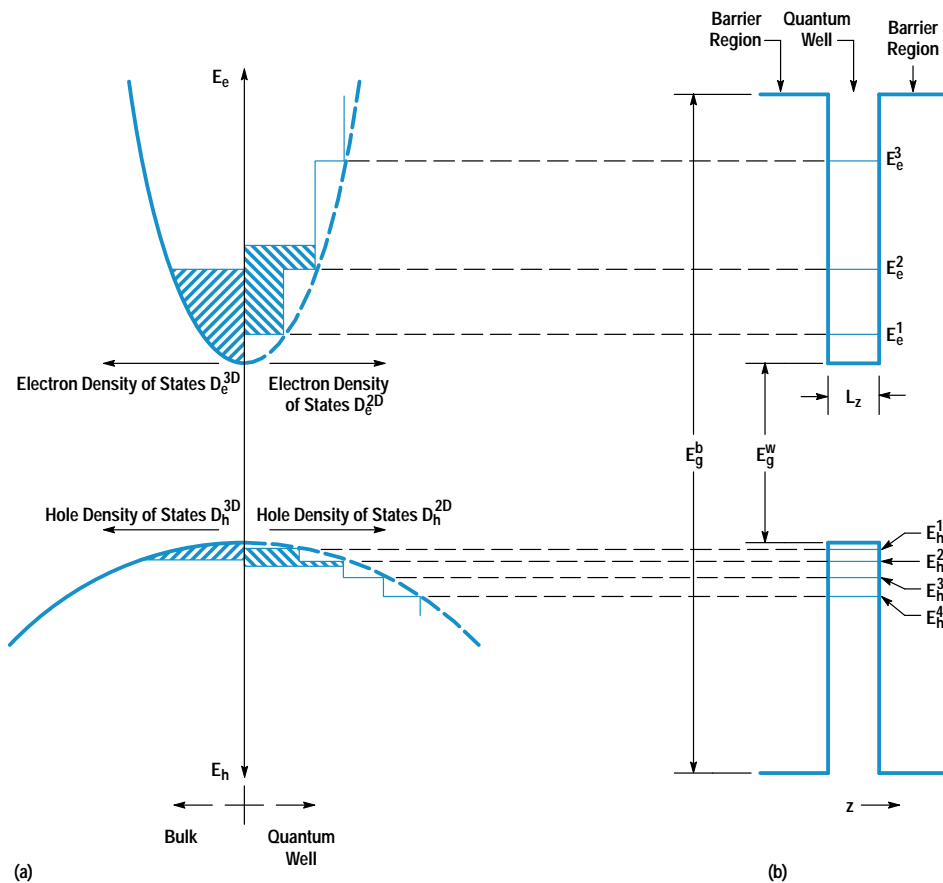


Fig. 3. (a) Parabolic and step density of states for bulk semiconductor (left of line) and quantum well (right of line). For a given volume density of carriers, electrons fill up to a greater depth for the quantum well case (right of line). (b) Discrete electron and hole energies from restricted z motion in a quantum well of thickness L_z . We have omitted the presence of a degenerate light hole band for this illustration.

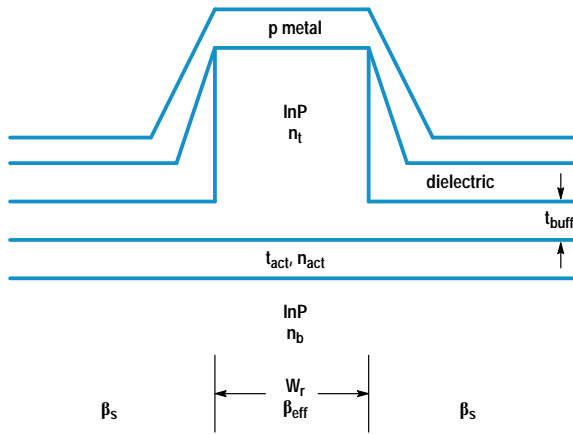
electrons and holes.⁴ Fig. 3 illustrates these observations for both bulk and quantum well semiconductor structures. Fig. 3a shows (hatched regions) the same volume density of electrons (and holes) distributed in energy space for bulk (left of line) and quantum well (right of line) structures. The electrons fill up to the available states and reach a higher energy for a quantum well than for a bulk active layer. It is this high energy state occupancy feature that allows a broad wavelength range of gain using quantum well active regions. Quantum well composition (which fixes the gap energy in the well region, E_g^w) and thickness (L_z), together with barrier region composition (which fixes the gap energy in the barrier region, E_g^b) determine the positions of the discrete levels E_e^1, E_e^2, \dots (see Fig. 3b). Level E_e^1 determines the long-wavelength end of the gain spectrum. The short-wavelength (or higher-energy) end of the gain spectrum is determined by the loss of electron confinement in the quantum wells. This loss of electron confinement is primarily determined by the barrier energy gap E_g^b . The upshot is that one needs to pick carefully the barrier material (for E_g^b), the quantum well material (for E_g^w), and the thickness L_z to ensure a properly wavelength-centered and sufficiently broad gain spectrum to fit the instrument need. In practice, the modal gain provided by a single quantum well is quite modest, so multiple quantum wells are used in parallel to achieve the requisite gain.

OMVPE Growth

Organometallic vapor phase epitaxy (OMVPE) dominates contemporary production of the quaternary compound semiconductor GaInAsP because of its relative simplicity, high yields, and scalability to large-area production. The GaInAsP material system has been studied since the early seventies

when it was realized that compositions lattice-matched to InP substrates would produce devices important for the then-incipient fiber-optic communication systems. OMVPE uses group III organometallic compounds such as triethylgallium (TEGa) or trimethylindium (TMIn, both metal alkyls) and hydrides of the group V elements, such as AsH_3 and PH_3 , as source materials for the vapor deposition. Vapors of the metal alkyls are entrained in a carrier gas, usually hydrogen, and transported to the heated substrate. The organometallics readily crack into single metal atoms and ethane or methane chains. The metal deposits on the growing surface, and the hydrocarbon chains are swept away in the carrier stream. Similarly, the hydrides also crack thermally, depositing only the group V atoms. A nearly perfect 1:1 stoichiometry of group V to group III atoms is achieved in the solid because the crystal strongly rejects excess group V atoms, which are volatile enough to evaporate.

The deposition zone design must incorporate several critical requirements. The substrate temperature must be uniform and tightly controlled since the As/P solid ratio is highly temperature-sensitive. The fluid dynamics must be controlled to deliver uniform amounts of precursor chemical to all parts of the substrate, and to compensate for any downstream depletion. Finally, turbulent flow streams defeat abrupt gas composition changes injected by the precision gas switching manifold and must be designed out. The laser diodes for the tunable source require precise control of the composition, thickness, and interfaces of nearly 20 epitaxial layers. The ratios of the four main gas constituents control the epitaxial GaInAsP composition, and the total metal alkyl concentration determines the epitaxial growth rate. Abrupt changes in



Want Small (Θ_{\perp} and Θ_{\parallel}), I_{th} , and High η_d

Optical Design

1. t_{act} , n_{act} , and n_t determine β_{eff} and Θ_{\perp} .
2. t_{buff} determines β_s .
3. β_{eff} , β_s , and W_r Determine Θ_{\parallel} .

Electrical Design

1. Want t_{buff} thin for small I_{th}
2. If $t_{buff} = 0$, optical loss is high, I_{th} increases, η_d decreases.
3. Free-carrier plasma causes lateral optical spread and reduces η_d at high currents.

Fig. 4. Ridge waveguide laser design issues. β_{eff} and β_s are the optical propagation constants for equivalent slab waveguides whose layers are the same as in the ridge and side regions of the device, respectively.

composition are achieved by rapidly switching the gas composition. Slow variations in the metal alkyl vapor ratios and hydride gas flow produce gradually graded material. In all cases, the epitaxial layer must remain lattice-matched to the InP substrate to within 2 parts in 10^4 to suppress dislocation formation. This requires precise control over the alkyl temperature ($\leq 0.1^\circ\text{C}$ variation), carrier gas flow, and the system pressure at several points.

The use of TMIn introduces another control complication. Unlike other commonly used metal alkyls, which are liquid over practical temperature ranges, TMIn is a solid. The concentration of the TMIn vapor sublimed into the gas stream varies (often unpredictably) with the solid surface area and the source lifetime. The TMIn vapor concentration in the hydrogen carrier gas must be constantly measured and controlled throughout the deposition cycle. By timing the transit of an ultrasound pulse through a real-time sample of the TMIn-hydrogen mixture, TMIn concentration to within 1 part in 10^5 can be determined.

Finally, small interfacial composition transients generate massive dislocation networks that destroy device performance. By controlling the temperatures, pressures, flows, and gas switching timings, essentially perfect interfaces can be formed. This allows growth of quaternary quantum wells as thin as 25\AA .

Ridge Laser Design Issues

The final device requires relatively small far-field divergence angles (Θ_{\perp} and Θ_{\parallel}), a small value of I_{th} and a high value for the differential quantum efficiency (η_d). Thickness (t_{act}) and effective index (n_{act}) of the active layer together with the refractive indexes of the top (n_t) and bottom (n_b) buffer regions determine β_{eff} and in turn control the angle Θ_{\perp} (see Fig. 4). (β_{eff} is the optical propagation constant for an equivalent slab waveguide whose layers are the same as the ridge part of the device.) The thickness (t_{buff}) of the buffer layer in the field and the width of the ridge (W_r) determine the angle Θ_{\parallel} . The thickness (t_{buff}) determines the size of the index discontinuity between the ridge and the field. A low threshold current is achieved by minimizing waste of carriers (to unnecessary lateral current spreading into the field regions) and by shielding the optical field from metal losses by a sufficiently thick dielectric layer. By judicious choice of dimensions these efficiency degrading current spreading effects can be minimized to obtain an extremely reliable device.

Once threshold (sufficient gain to account for all losses) is reached, any extra current produces lasing photons. These photons still face losses from various physical mechanisms: absorption in pumped and unpumped regions, scattering from defects, metal absorption losses, and useful light output from the end mirrors. The differential quantum efficiency can be expressed as:

$$\eta_d = \eta_i \left(\frac{\alpha_{mir}}{\alpha_{mir} + \alpha_{int}} \right),$$

where η_i is the internal quantum efficiency indicating the fraction of injected carriers converted to photons, α_{mir} is the loss resulting from light emitted from an end mirror, and α_{int} is the loss resulting from various internal factors. Both non-radiative recombination at surfaces and defects and Auger recombination[†] make η_i less than 100%. Since α_{mir} signifies useful output, one needs to keep α_{int} to a tolerable minimum to achieve a high η_d . For a semiconductor laser of length L_d and facet reflectivity R ,

$$\alpha_{mir} = (1/L_d) \ln(1/R).$$

A value of L_d chosen to make $\alpha_{mir} = \alpha_{int}$ maximizes the output power. Factors dictated by instrument operation determine the actual device length.

Device Fabrication and Testing

Starting with a proper structure epitaxially grown on n-type InP substrate, a mask for the ridge is defined photolithographically. Using this mask, ridges of the chosen width and height are etched using a methane/hydrogen reactive ion etch.⁶ A dielectric layer is deposited all over and selectively cleared from the ridge tops using a self-aligned photoresist process. Fig. 5 is an SEM cross-section showing photoresist on the sides, selectively protecting the dielectric layer that covers the entire top surface. Following this step, the dielectric layer is etched off the ridge top and the photoresist is removed from the field (see Fig. 6). A p contact/metal combination is deposited, covering the exposed ridge tops and the dielectric in the field. A thick gold pad is plated over the p metals to act as a heat spreader and as a bond pad. The wafer is thinned and an n contact metallization is deposited. Following a high-temperature contact alloying step the wafer

[†] Very briefly, Auger recombination⁵ is a nonradiative and therefore lossy process that involves four particles: either three electrons and one hole or three holes and one electron. The Auger process is especially important in determining the temperature dependence of threshold current and η_i in long-wavelength semiconductor lasers such as ours.

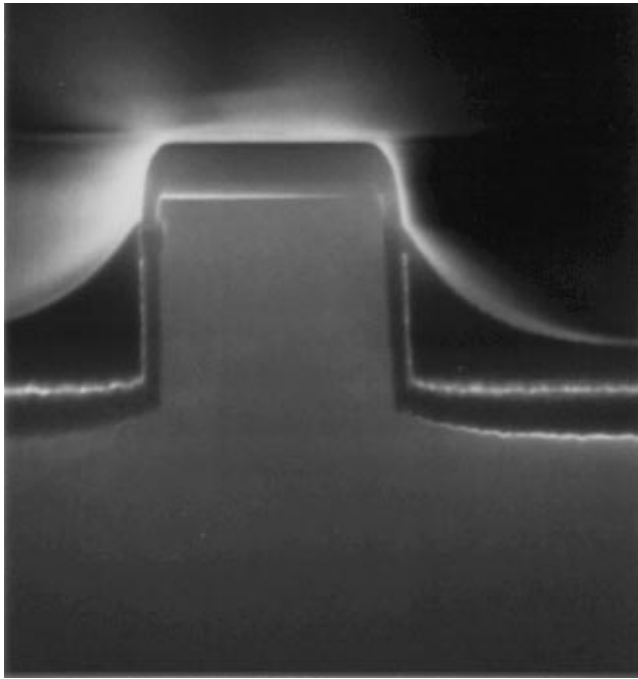


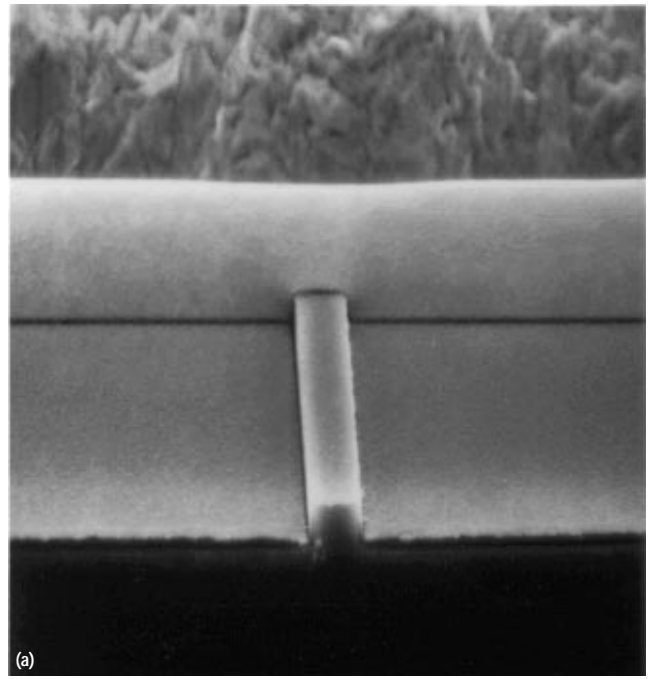
Fig. 5. Scanning electron microscope cross section of a ridge waveguide laser after exposure of ridge top with photoresist covering the oxide in the field.

is cleaved into bars for device testing. Fig. 7a is an SEM section of a completed device showing the ridge, a device facet, and the plated gold pad on top. Fig. 7b shows details of the device cross section with the active and contact layers clearly delineated.

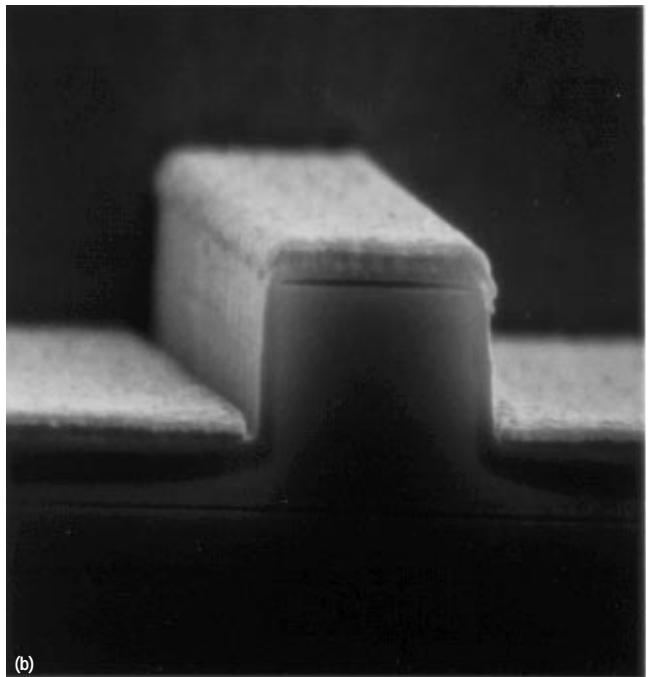
Devices are first pulse tested in bar form to get an idea of their operation before die-attachment onto a heat sink. Devices 500 micrometers long have typical thresholds in the



Fig. 6. SEM cross section of a ridge waveguide laser after removal of the dielectric from the ridge top and photoresist from the field.



(a)



(b)

Fig. 7. (a) SEM section of a completed ridge laser showing the ridge and the plated gold. (b) SEM section of a ridge laser facet delineating the active and contact layers.

low 20-mA range with excellent slope efficiency and low divergence angles. Fig. 8 shows pulsed L-I and I-V characteristics, where L is light power output. Fig. 9 shows the far-field divergence angles perpendicular (Θ_{\perp}) and parallel (Θ_{\parallel}) to the plane of the device at different currents.

Device Reliability

A number of factors go into ensuring the reliability of our devices. To project device lifetimes under operational conditions, batches of devices die-attached to a suitable heat sink are subjected to elevated temperatures and a high bias current over many thousand hours. Periodically threshold

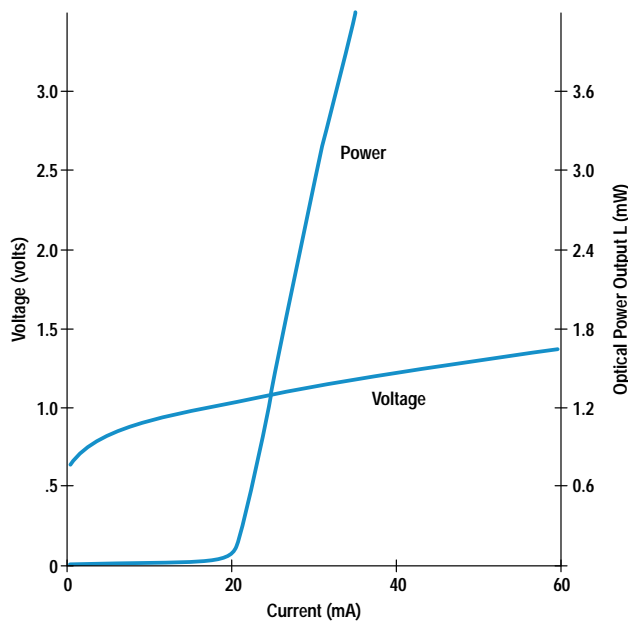


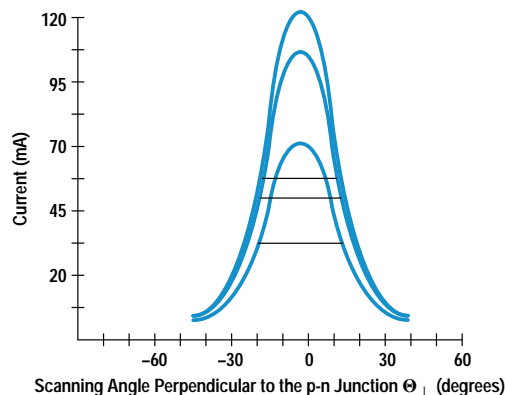
Fig. 8. Pulsed L-I (optical power output versus current) and I-V curves for a representative 1550-nm ridge waveguide laser.

current, power, and differential quantum efficiency are measured. The change in these parameters for devices stressed at different temperatures can be used to extract an activation energy for the principal failure mechanism. Device lifetime can then be predicted for normal operating conditions.

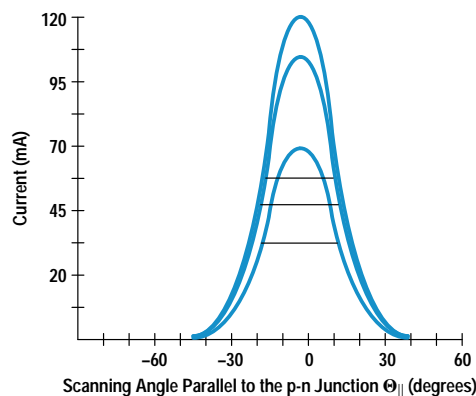
External-Cavity Operation

Completed individual devices are mounted on a heat sink. One facet is antireflection coated with a broadband multi-layer coating.³ The quality of this coating determines the suppression level of output power variations (from parasitic reflections), and ≤ 1 dB at the highest power levels of operation is achievable. With one of these devices properly aligned in an external cavity (see Fig. 10) we can generate a wavelength tuning curve at any operating current. Fig. 11 shows the power output as a function of wavelength for a representative device tested in an external cavity at an operating current of ≈ 120 mA.

Devices show > 0 dBm output power (in a collimated beam) over the wavelength window 1465 to 1625 nm and put out > 10 dBm over a smaller window, 1505 to 1615 nm. A single-mode fiber provides the output of the instrument (HP 8168C). With a reflection suppressing isolator included, these raw power output and tuning numbers are degraded somewhat.



Peak Current (mA)	Θ_{\perp} FWHM (Degrees)
70	32.6
100	32.7
120	32.7



Peak Current (mA)	Θ_{\parallel} FWHM (Degrees)
70	23.4
100	23.5
120	23.9

Fig. 9. Far-field divergence angles perpendicular (Θ_{\perp}) and parallel (Θ_{\parallel}) to the device junction plane.

Nevertheless, these new custom ridge waveguide laser chips still provide significant increases in the power output and tuning window for the new instrument. The HP 8168C covers the range 1470 to 1590 nm with power increased by 8 dB and tuning window widened by a factor of two over the HP 8168A. Offering higher power (+2.5 dBm) in the range 1520

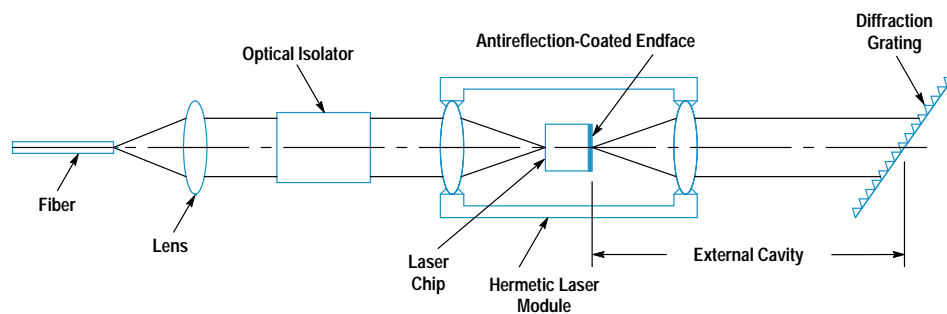


Fig. 10. Schematic of a laboratory grating-tuned external-cavity test setup.

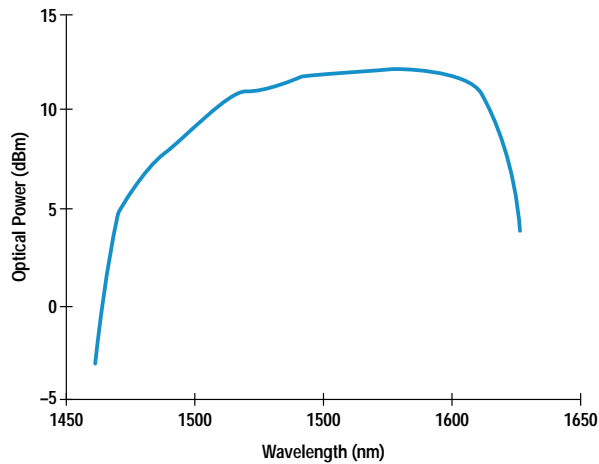


Fig. 11. Power output as a function of wavelength for a representative ridge laser in an external cavity.

to 1565 nm, this instrument is expected to be very useful for saturation measurements of erbium-doped fiber amplifier (EDFA) systems.

Summary

A multi-quantum-well ridge waveguide laser enhanced for use in a grating-tuned external-cavity source has been developed. The device offers higher output power and wider tunability in the new HP 8168C tunable laser source. This tunable optical source will allow simple testing of components for wavelength division multiplexing (WDM) as well as complete testing of EDFA systems. The core technology will allow the

fabrication of other custom light sources in the wavelength window 1200 to 1700 nm.

Acknowledgments

The authors would specially like to thank Rose Twist for assistance in process development and device fabrication and Pamela Langhoff for assistance with epitaxial growth. Other people who have contributed to this project include: Jean Norman, Gary Trott, Joan Henderson, Mimi Planting, Nance Andring, Kari Salomaa, Nancy Wandrey, Deborah Sowers, and Roger Jungerman. We would like to express our appreciation for managerial support from Rick Trutna, Waguhi Ishak, Kent Carey, Susan Sloan, Bob Bray, Jun Amano, and Ron Moon.

References

1. B. Maisenbacher, E. Leckel, R. Jahn, and M. Pott, "Tunable Laser Sources for Optical Amplifier Testing," *Hewlett-Packard Journal*, Vol. 44, no. 1, February 1993, pp. 11-19.
2. I.P. Kaminow, R.E. Nahory, M.A. Pollack, L.W. Stulz, and J.C. Dewinter, "Single-mode CW ridge-waveguide laser emitting at 1.55 μm ," *Electronics Letters*, Vol. 15, 1979, pp. 763-765.
3. R.L. Jungerman, D.M. Braun, and K.K. Salomaa, "Dual-Output Laser Module for a Tunable Laser Source," *Hewlett-Packard Journal*, Vol. 44, no. 1, February 1993, pp. 32-34.
4. C. Weisbuch and B. Vinter, *Quantum Semiconductor Structures*, Academic Press, 1991, p. 21.
5. G.P. Agrawal and N.K. Dutta, *Long-Wavelength Semiconductor Lasers*, Van Nostrand Reinhold, 1986, Chapter 3.
6. U. Niggebrugge, M. Klug, and G. Garus, "A novel process for reactive ion etching on InP, using CH_4/H_2 ," *Institute of Physics Conference Series*, no. 79, 1986, pp. 367-372.